TENSILE AND FATIGUE PROPERTIES OF HOT ROLLED STEELS FOR LONGITUDINAL GIRDERS

[1] Gatti, M. C. A., mcgatti@sc.usp.br
[2] Garcia, A., Ailton.garcia@gm.com
[1] Tarpani, J. R., jrpan@sc.usp.br
[1] Spinelli, D., dspinell@sc.usp.br

[1] Department of Materials Engineering, São Carlos School of Engineering University of São Paulo, Av. Trabalhador São-Carlense, 400, São Carlos 13566-590, SP, Brazil
[2] Department of Materials of General Motors of Brazil, Av. Goiás, 1805, São Paulo 09550-900, São Caetano do Sul, SP, Brazil

Abstract. *The purpose of this work was to investigate the mechanical behavior of hot-rolled NBR10 LNE 23 low carbon steel and DP 600 dual-phase steel designed for cold drawing of longitudinal girders for automotive applications. The properties of interest were determined from monotonic tensile tests and strain control fatigue tests carried out at room temperature. Dual-phase DP 600 steel showed superior tensile behavior of the following properties: tensile strength, yield strength, tensile ratio parameters, resistance coefficient and strain hardening exponent. NBR 6656 LNE 23 steel presented higher tensile parameters of elongation, area reduction and anisotropy. Cyclic stress-strain stress-life curves and stress-life relationships were obtained for both steels in the transverse rolling direction. Fatigue crack propagation tests were also conducted at room temperature under constant-amplitude loading and R=0.1. The mean values of the threshold stress intensity factor in the transverse rolling direction were 6.25 MPa.*$m^{1/2}$ *for NBR 6656 LNE 23 steel, and 5.02 MPa.*$m^{1/2}$ *for the dual phase DP 600 steel. The Paris-Erdogan relationship for the fatigue crack growth was* $da/dN = 2.98.10^{-10}(\Delta K)^{4.02}$ *mm/cycle for NBR 6656 LNE 23 steel and* $da/dN = 3.33.10^{-8}(\Delta K)^{2.58}$ *mm/cycle for DP600 dual-phase steel.*

Keywords: *Hot rolled steels, Monotonic properties, Low cycle fatigue, Fatigue crack propagation, Regime I and II.*

1. INTRODUCTION

Microalloyed steels are known as high-strength low-alloy (HSLA) steels and usually present good mechanical properties at room temperature. The need to obtain both higher mechanical strength and good formability steels has led to the development of another class, called dual-phase steels, which can be produced simply by subjecting them to a suitable heat treatment involving cooling from the dual-phase austenitic-ferritic field ($\alpha+\gamma$). The term dual-phase refers to the predominance of the two-phase microstructure of ferrite and martensite at room temperature. These steels exhibit significant ductility, as well as good formability, high work hardening rates, and high fatigue strength (Speich, 1994).

Microalloyed steels, otherwise, contain stabilizers elements of carbon and nitrogen such as niobium, titanium, vanadium and aluminum, with additions of up to 0.1%. They also present carbides, nitrides and carbon nitrides finely dispersed in the ferritic matrix, which favor hardening of the material and improve its mechanical properties. These steels are employed in parts whose formability is critical and special requirements of mechanical properties and weldability are fundamental, such as girders and cross beams (Garcia, 2003).

The purpose of this work was to investigate two different hot-rolled steels, one microalloyed and another dual-phase, from the standpoint of their tensile, formability, and low-cycle fatigue properties, as well as fatigue crack propagation behavior, for applications in girders cars.

2. MATERIALS AND METHODS

2.1 Materials

Both hot-rolled steels were studied, a microalloy (NBR 6656 LNE 23) and a dual-phase (DP600), for cold stamping operations. The thickness of plates were approximately 3 mm. Table 1 provides the chemical composition, in weight percent, of the materials investigated.

Table 1. Chemical composition of the steels (in wt. %).

Materials	C	Si	Mn	P	S	Al	Ni	Cr	Mo	Nb	Ti
LNE 23	0.050	0.005	0.290	0.012	0.014	0.044	0.01	0.01	0.001	0.001	0.001
DP600	0.056	1.12	1.22	0.015	0.004	0.043	0.01	0.10	-	0.002	0.002

2.2. Tensile Tests

Tensile tests were conducted according to ASTM E8M – 09. The specimens were machined in longitudinal, 45^o and transverse directions. Were tested three specimens for directions. Fig. 1 illustrates the geometry and dimensions of the tensile tests specimens.

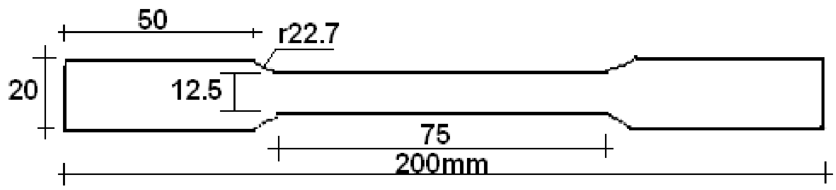

Figure 1. Geometry and dimensions of the test specimens. Dimensions in mm.

The tests to determine the plastic strain ratio (r) and strain hardening monotonic exponent (n) were performed according to the ASTM E517 - 06 and ASTM E646 - 07, respectively.

All tests were performed at room temperature, in an MTS-810 servo-hydraulic testing machine of 100 kN capacity, with crosshead speed of 0.5 mm/min up to 0.5% of strain, and increasing to 5 mm/min above this strain.

2.3. Low-Cycle Fatigue Tests

Figure 2a displays the geometry and dimensions of the test specimens used in low-cycle fatigue tests to obtain strain-life relationships. Previous studies have shown that this geometry tends to minimize the lack of alignment of samples in tension-compression fatigue tests at a deformation rate of R = - 1 (Milan et al., 2001). The specimens were tested in the loading direction perpendicular to the rolling direction.

The tests were carried out at room temperature according to ASTM E606 – 04, in a 100 kN capacity MTS-810 servo-hydraulic testing machine (Fig. 2b), under frequencies ranging from 0.5 Hz to 2 Hz, sinusoidal strain wave and total strain amplitudes varying from 0.10% to 0.40%. A 50% drop in load compared to the reference cycle (cycle 50) was adopted as the criterion of failure.

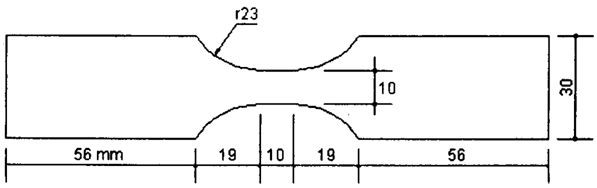

(a)

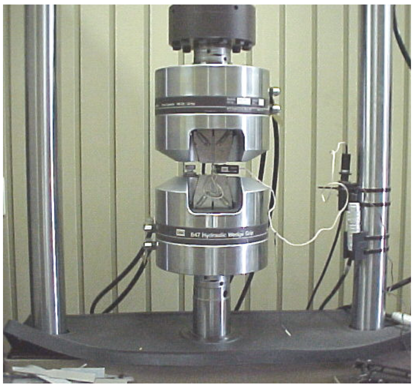

(b)

Figure 2. (a) Geometry and dimensions in mm of the fatigue specimen, and (b) detail of the test specimen fixed in the grips of the MTS testing machine.

The strain-controlled fatigue testing programs were conducted with 50%-75% replication, as recommended in the ASTM E 739-10 for design allowable data type of test.

2.4 Fatigue Crack Propagation Tests

Figure 3a illustrates the geometry and dimensions of the compact tension specimens, C(T), used in the fatigue crack propagation testing to obtain da/dN-ΔK curves in Regimes I and II of fatigue crack propagation. Two specimens of steels were machined and tested in TL direction.

The tests were carried out at room temperature according to the ASTM E647-08, using a 100 kN capacity MTS-810 servo-hydraulic testing machine (Fig. 3b). The specimens used to determine Paris-Erdogan equation (1960) were tested in controlled loading, loading ratio R = 0.1, under a constant-amplitude sinusoidal wave of 20 Hz. Crack growth rates as a function of the variation of the stress intensity factor was determined by a computer program for data reduction by the seven point increment polynomial technique.

The compact tension C(T) specimens used to determine the fatigue crack growth threshold (ΔK_{th}) were tested using K-decreasing procedure for da/dN < 10^{-8} mm/cycle and met the normalized K-gradient, C=1/K x dK/da = -0.079mm^{-1} and a continuously decreasing load at a loading rate of R = 0.1. A constant-amplitude sinusoidal load wave of 20 Hz was imposed to the system. The da/dN versus ΔK data points were determined by the secant method. The value of ΔK_{th} was obtained by the best-fit straight line from a linear regression of log da/dN versus log ΔK, using a minimum of five da/dN, ΔK data points of approximately equal spacing between growth rates of 10^{-9} and 10^{-10} m/cycle. The intercept of the above fitted straight line with to a growth rate of 10^{-10} m/cycle gave the value of ΔK_{th} according to the operational definition of the ASTM E647-08 test method.

The compliance method of crack size monitoring was employed to measure the fatigue crack growth rate of tests (Donald and Schmidt, 1980).

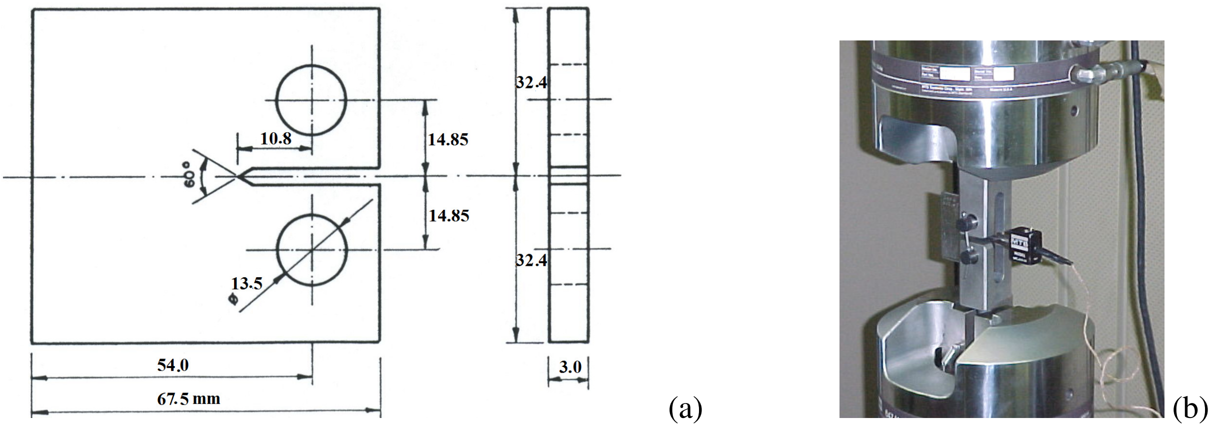

Figure 3. (a) C(T) specimen. Dimensions in mm and (b) detail of the specimen fixed in the grips of MTS testing machine.

2.5 Fractographic Analysis

Fractographic analyses were performed on a scanning electron microscope (SEM), using the secondary electron technique to analyze the fracture surfaces of the steels presented in the regime II of crack growth for low cycle fatigue and in the regimes A and B of fatigue crack propagation (Supra, 2003).

3. RESULTS AND DISCUSSION

3.1 Tensile Tests

Table 2 presents the average values of results obtained of the parameters of monotonic properties.

The parameters of tensile strength of LNE 23 steel are slightly higher in the direction diagonal to rolling plate, while those of the DP 600 dual-phase steel are slightly higher in the rolling direction.

The value of the mean normal anisotropy decreased in the DP 600 steel as the parameters of tensile strength increased, indicating a reduction in the steel's cold drawing ability in response to the increase in the degree of the tensile strength parameters.

Table 2. Average values of parameters of monotonic properties.

Materials	**LNE 23**			**DP 600**		
	L	**LT**	**T**	**L**	**LT**	**T**
S_r (MPa)	347	348	347	637	635	635
$S_{e(0,2\%)}$ (MPa)	248	265	256	418	408	418
$e_{t(50mm)}$ (%)	41	43	43	26	24	25
E (MPa)	208000	219000	217000	209000	205000	207000
RA (%)	76	78	76	68	68	67
n	0.14	0.13	0.13	0.17	0.17	0.16
K	532.09	526.54	518.13	1002.58	1008.51	1009.31
r(0º,45º,90º)	0.86	0.93	0.94	0.80	0.97	0.81
r_m	0.92			0.89		
Δr	-0.03			-0.17		

S_r = ultimate tensile strength
$S_{e(0,2\%)}$ = yield strength at 0.2% of strain
e_t = total elongation measured in 50 mm
RA = reduction of area
n = strain hardening exponent
K = strength coefficient
E = modulus of elasticity
r = plastic strain ratio
r_m = normal anisotropy
Δr = planar anisotropy

3.2 Low-Cycle Fatigue Tests

Table 3 presents the results of the low-cycle fatigue parameters obtained for both steels in the transverse direction (T). Fig. 5 presents the strain-life curves of both materials.

Table 3. Low-cycle fatigue properties of the LNE 23 and DP 600 (T) steels.

Materials	**Results Fatigue**							
	n'	**K'**	**σ_e' (MPa)**	**b**	**σ'_f (MPa)**	**ε'_f**	**c**	**$2N_t$**
LNE 23	0.26	1129	225	-0.12	670	0.10	-0.42	78054
DP 600	0.07	732	465	-0.08	930	3.95	-0.92	3545

n' = cyclic strain hardening exponent
K' = cyclic strength coefficient
σ_e' = cyclic yield stress
σ'_f = fatigue strength coefficient
c = fatigue ductility exponent
ε'_f = fatigue ductility coefficient
b = fatigue strength exponent
$2N_f$ = reversals to failure
$2N_t$ = transition fatigue life

As depicted in Tab. 3 and Fig. 4, the DP 600 dual-phase steel presented higher low-cycle fatigue results compared to the LNE 23 steel.

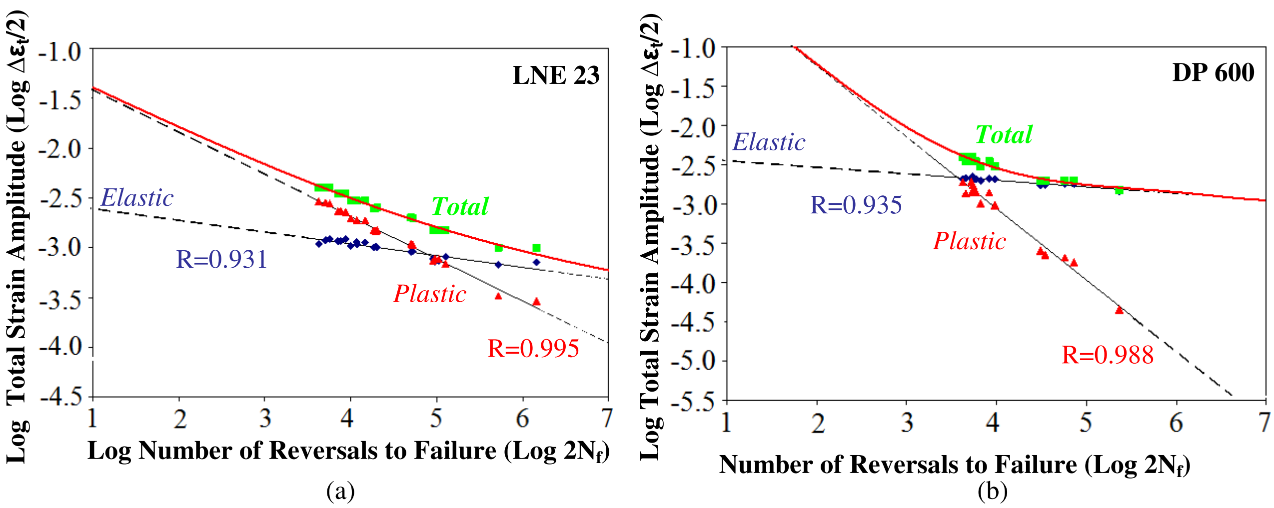

Figure 4. Strain-life curves of: (a) LNE 23, and (b) DP 600 steels.

The fatigue-life relationships for both steels are presented in Tab. 4.

Table 4. Fatigue life relarionships.

Material	$\Delta\varepsilon_t/2= \sigma'_f.(2N_f)^b/E + \varepsilon'_f.(2N_f)^c$
LNE 23	$\frac{\Delta\varepsilon_t}{2} = 0.003.(2N_f)^{-0.12} + 0.10.(2N_f)^{-0.42}$
DP 600	$\frac{\Delta\varepsilon_t}{2} = 0.004.(2N_f)^{-0.08} + 3.95.(2N_f)^{-0.92}$

3.3 Fatigue Crack Propagation Tests

The fatigue crack propagation rate curves as a function of the stress intensity factor range, da/dN x ΔK, used for the determination the Paris-Erdogan equations of the LNE 23 and dual-phase DP 600 steels are depicted in Figs. 5 and 6, respectively. The blue dots indicate the results obtained in the tests, while the red lines represent the straight line used to determine the coefficient C and exponent m of Paris-Erdogan equations of steels.

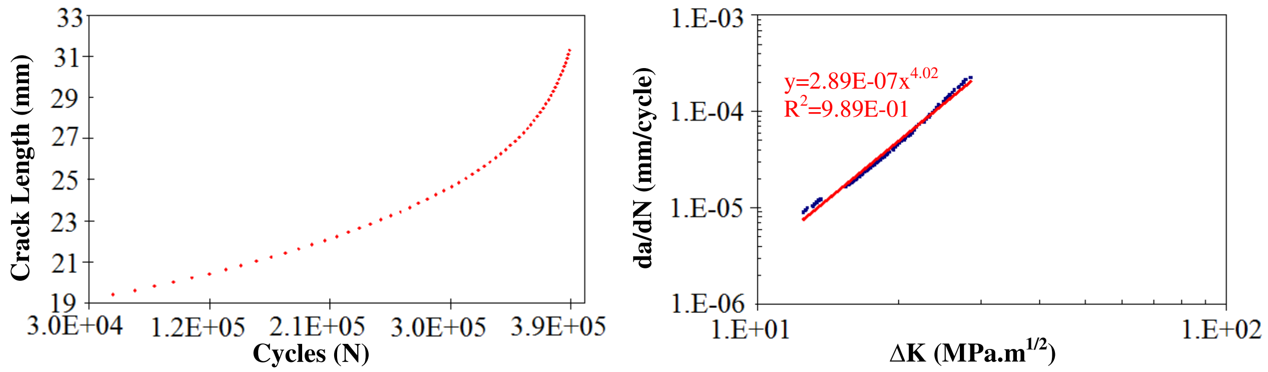

(a) (b)

Figure 5. (a) **a** versus **N** date points obtained experimentally for the LNE 23 steel, (b) da/dN versus ΔK in regime A to determine the coefficient C and exponent m of Paris-Erdogan equation.

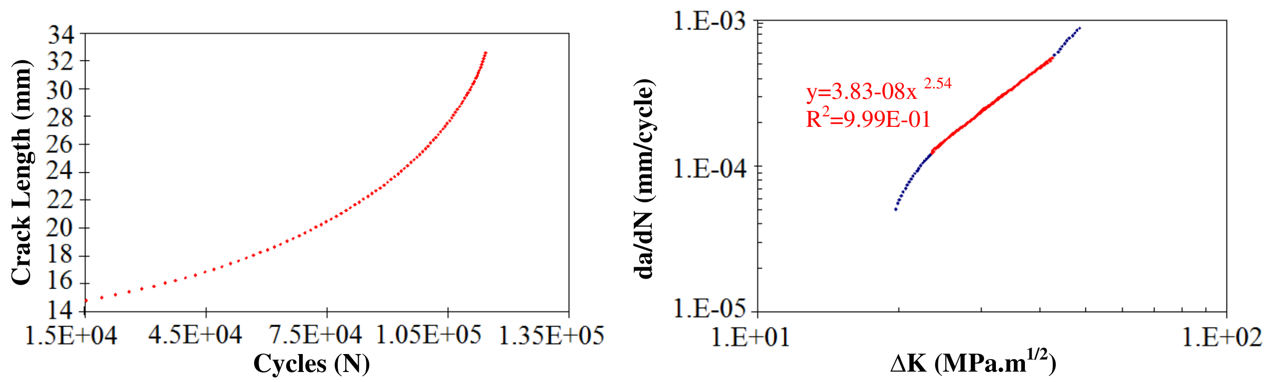

(a) (b)

Figure 6. (a) **a** versus **N** date points obtained experimentally for the DP 600 steel, (b) da/dN versus ΔK in regime A to determine the coefficient C and exponent m of Paris-Erdogan equation.

Figures 7 and 8 present the results of **a** versus **N** and da/dN versus ΔK which were used to determine the threshold stress intensity factor (ΔK_{th}) for the LNE 23 and dual-phase DP 600 steels, respectively. All the values obtained with the force shedding during the K-decreasing test are shown in blue and red. The results showed in red dots were used for the determination of the threshold stress intensity factor (ΔK_{th}), whose procedure was performed according to ASTM E647-08.

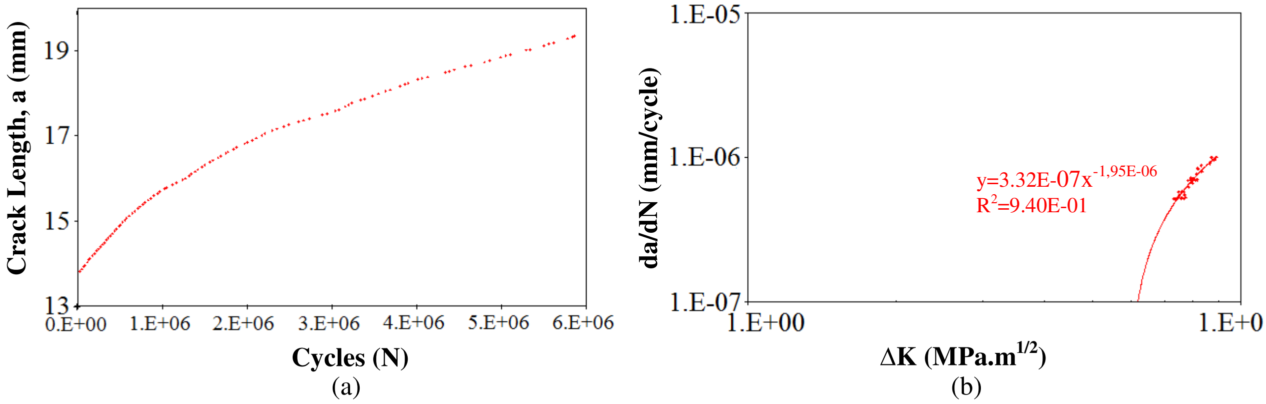

Figure 7. (a) **a** versus **N** data points obtained from ΔP shedding decreasing loads to find de threshold stress intensity value, (b) Results of da/dN versus ΔK obtained from ΔP shedding decreasing loads for LNE 23 steel.

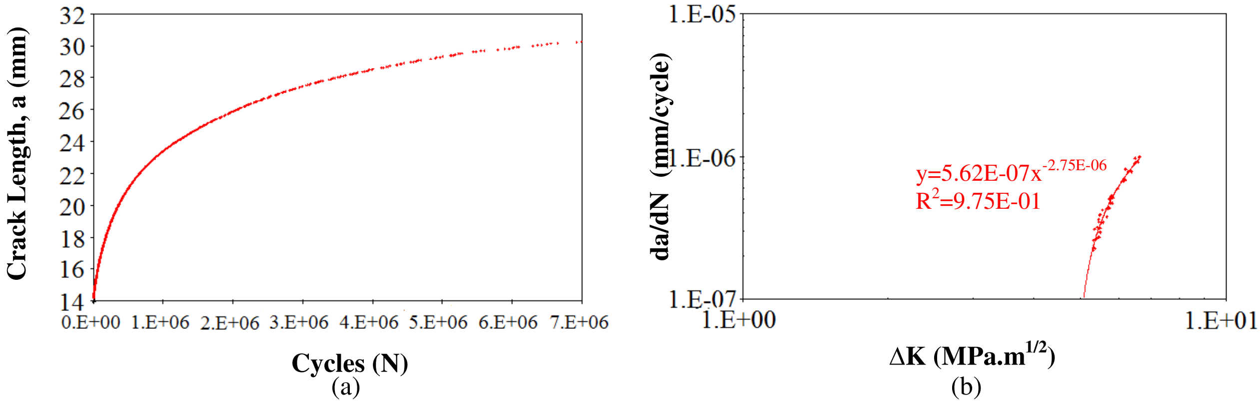

Figure 8. (a) **a** versus **N** data points obtained from ΔP shedding decreasing loads to find de threshold stress intensity value, (b) Results of da/dN versus ΔK obtained from ΔP shedding decreasing loads for DP 600 steel.

The Figure 9 show the results of the best-fit straight line from a linear regression of log da/dN versus log ΔK using a minimum of five da/dN, ΔK data points of approximately equal spacing between growth rates of 10^{-6} to 10^{-7} mm/cycle. The ΔK-values that correspond to a growth rate of 10^{-7} mm/cycle give the values of ΔK_{th} of steels according to the operational definition of the method ASTM E647-08.

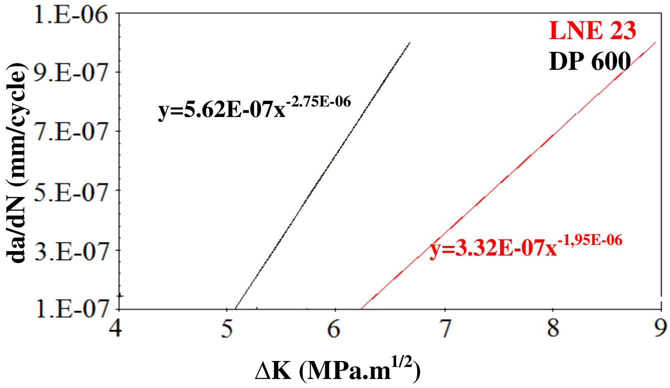

Figure 9. Best fit straight line for the determination of ΔK_{th} values.

Values of the threshold stress intensity factor and the Paris-Erdogan equation for both steels are presented in Tab. 5.

Table 5. Threshold stress intensity factor and Paris-Erdogan equation.

Material	Threshold Stress Intensity Factor ΔK_{th}	Paris-Erdogan equation $da/dN = C.\Delta K^m$
LNE 23	6.25	$\frac{da}{dN} = 2.89.10^{-10}.\Delta K^{4.02}$
DP 600	5.02	$\frac{da}{dN} = 3.83.10^{-8}.\Delta K^{2.54}$
Obs: The Paris-Erdogan equations above give the crack growth rate da/dN in mm/cycle for ΔK in $MPa.m^{1/2}$ unit.		

The results showed in the Fig. 9 indicate that the LNE 23 steel is more resistant to fatigue crack propagation in the regime I and present a more great value of the threshold stress intensity factor (see Tab. 5). However an analysis of Paris-Erdogan regime reveals that the LNE 23 steel up to ΔK value of approximately 26 $MPa.m^{1/2}$ is still more resistant to fatigue crack propagation. Above this value, the DP 600 steel showed more resistant to fatigue crack propagation. This occurs because the LNE 23 steel presents a higher crack propagation gradient, i.e., m= 4.02, than the DP 600 steel, which is m= 2.52. This behavior can be seen in the Fig 10.

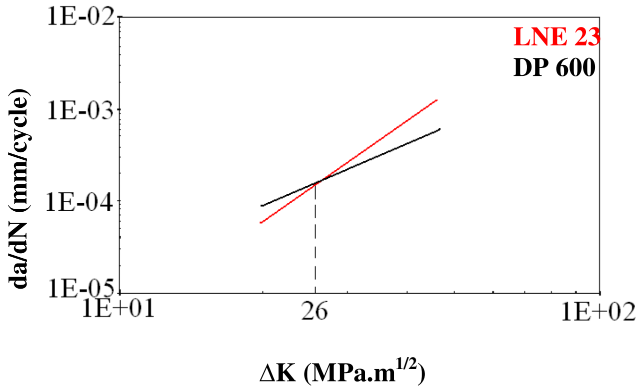

Figure 10. da/dN versus applied ΔK in regime II for the steels.

3.4 Results of the SEM Fractographics Analyses

Figure 11 shows the fracture surface observed in the stage II of Forsyth (1961) for two specimens tested in low-cycle fatigue testing, in approximately the same applied levels of total strain amplitude. The results show in the Fig. 11 indicates that the fracture surface presented essentially similar transgranular fracture surfaces behavior, showing well defined fine striations which characterize stage II of fatigue crack propagation of ductile materials.

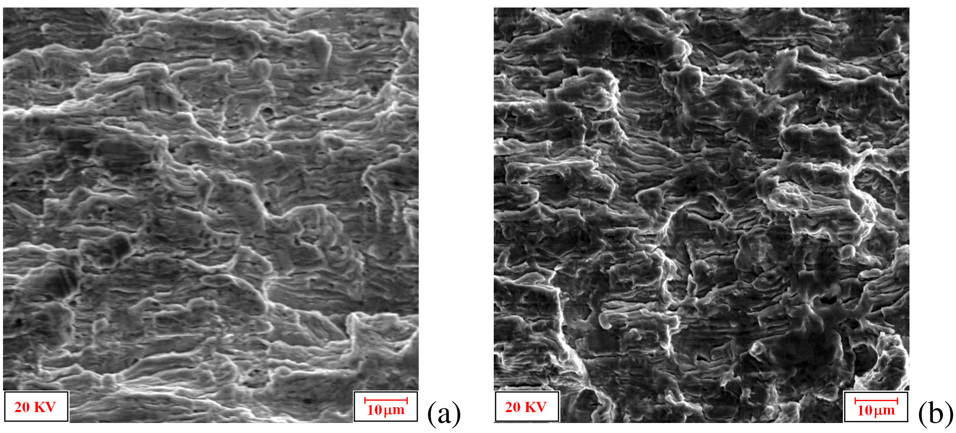

Figure 11. Low-cycle fatigue SEM fractographs: (a) $\Delta\varepsilon_t/2$= 0.40% for the LNE 23 steel specimen and (b) $\Delta\varepsilon_t/2$= 0.35% for the DP 600 steel specimen.

Some aspects of the fracture surfaces observed in the regime of fatigue crack propagation of the steels near to the threshold stress intensity factor ΔK_{th} and in Paris-Erdogan regime close to crack propagation rate of 10^{-4} mm/cycle are shown in Figs. 11 and 12.

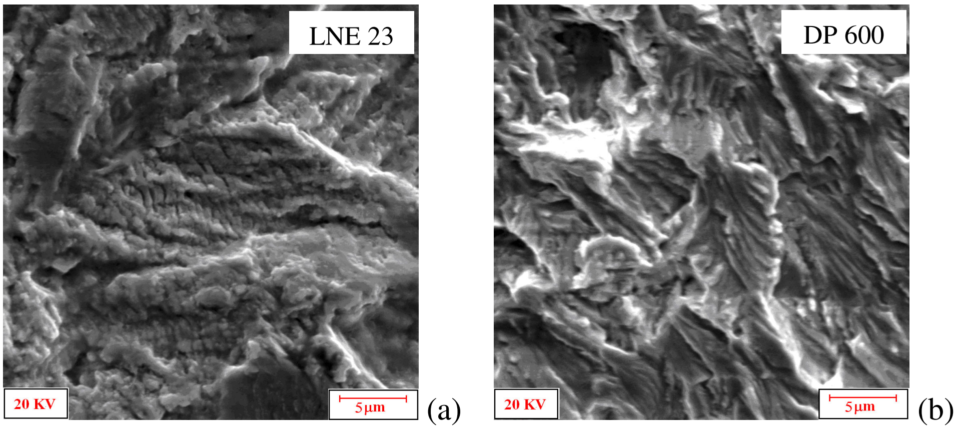

Figure 12. SEM fractographs taken in the regime I of fatigue crack propagation near-threshold: (a) $\Delta K \cong 7$ MPa.m$^{1/2}$ and (b) $\Delta K \cong 6$ MPa.m$^{1/2}$.

The dominant fracture mode in the regime of crack propagation of the fracture surfaces close to the threshold is transgranular, with minor undulations (peaks and valleys).

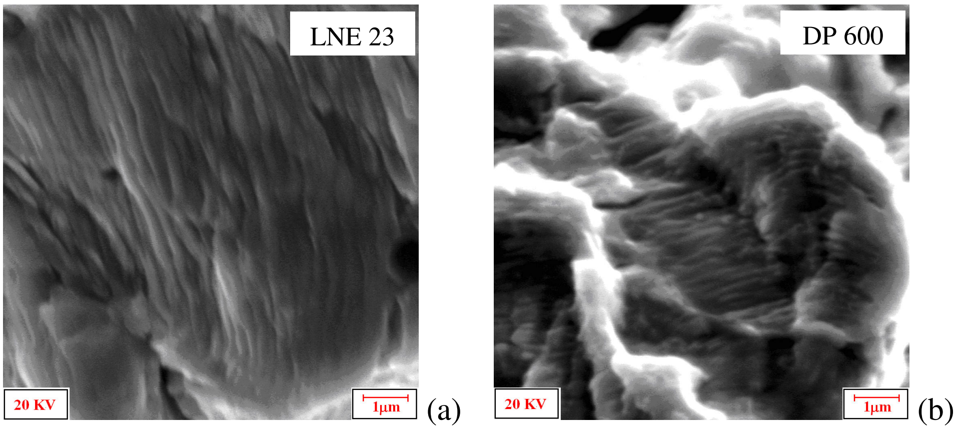

Figure 13. SEM fractographs observed in the regime II of fatigue crack propagation: (a) for $\Delta K \cong 28$ MPa.m$^{1/2}$, LNE 23 steel, and (b) for $\Delta K \cong 20$ MPa.m$^{1/2}$, DP 600 steel.

For crack growth rates in Paris-Erdogan regime, as show in Fig. 13, the fracture surfaces were found to be essentially transgranular, showing well defined striations. Irregular spaced secondary cracks can be observed, which characterize higher rates of fatigue crack propagation.

4. CONCLUSIONS

The DP 600 dual-phase steel presents superior tensile properties than the LNE 23 steel in terms of strength parameters such elastic ratio, strength coefficient and work-hardening exponent. On the other hand, the LNE 23 steel presents better performance in tensile than the DP 600 dual-phase steel in ductile parameters and anisotropy.

The DP 600 steel exhibits higher fatigue strength coefficient (σ'_f) and fatigue ductility coefficient (ε'_f) than the LNE 23 steel. This means that the fatigue strength of DP 600 dual-phase steel is higher than that of LNE 23 steel.

The LNE 23 steel has increased resistance to crack propagation in the regime I and in the Paris-Erdogan regime II until the value of ΔK~26 MPa.m$^{1/2}$. However, at ΔK values great than 26MPa.m$^{1/2}$ the inverse occurs and DP 600 steel shows greater resistance to crack propagation.

The predominant fracture mode in regime I of fatigue crack propagation near the threshold value (ΔK_{th}) for the steels is typically transgranular, with minor undulations (peaks and valleys). In Paris-Erdogan regime of fatigue crack propagation the fracture surfaces presented well defined fine striations which characterizing the high ductility of both steels.

5. ACKNOWLEDGMENTS

The authors acknowledge the financial support of the Brazilian research funding agencies CAPES (Proc. n^0 23038038434/2008-33) and FAPESP (Proc. n^0 02735-6) and General Motors of Brazil for donating the materials used in this work.

6. REFERENCES

Donald, J.K., Schmidt, D.W., 1980, "Computer-controlled stress intensity gradient technique for high rate fatigue crack growth testing", Journal of Testing and Evaluation, Vol.8, No.1**,** pp. 19-24.

Forsyth, P.J.E., 1961, "A two stage process of fatigue crack growth", Proceedings of the crack propagation symposium, Cranfield, England, pp. 76-94.

Garcia, A., 2003, "Mechanical properties of fatigue of hot rolled steels for longitudinal girders" (In Portuguese), Ms.C. Dissertation , University of São Paulo, São Carlos, S.P., Brazil, 125p.

Milan, M.T., Spinelli, D., Bose Filho, W.W., 2011, "Fatigue and monotonic properties of an interstitial free steel sheet (FMPIF)", International Journal of Fatigue, Vol. 23 pp. 129-133.

Paris P.C., Erdogan F., 1960, "Critical analysis of crack propagation laws", Journal of Basic Engineering, Vol. 85, pp. 528–534.

Speich, G.R., 1994, "Dual Phase Steels, In: Properties and selection: irons, and high performance alloys," Metals Handbook, Tenth Edition ASM International, Vol.1, pp. 424-429.

Suresh, S., 2003, "Fatigue of Materials", Second Edition, published by Cambridge University Press, reprinted with correction in 2003, pp. 335-342.

7. RESPONSIBILITY NOTICE

The authors are the only responsible for the printed material included in this paper.